IOPscience iopscience.iop.org

Home Search Collections Journals About Contact us My IOPscience

Reaction kinetics of nanostructured silicon carbide

This article has been downloaded from IOPscience. Please scroll down to see the full text article.

2008 J. Phys.: Condens. Matter 20 325216

(http://iopscience.iop.org/0953-8984/20/32/325216)

View the table of contents for this issue, or go to the journal homepage for more

Download details:
IP Address: 129.252.86.83
The article was downloaded on 29/05/2010 at 13:48

Please note that terms and conditions apply.

J. Phys.: Condens. Matter **20** (2008) 325216 (6pp) doi:10.1088/0953-8984/20/32/325216

Reaction kinetics of nanostructured silicon carbide

K L Wallis[1], J K Patyk[1,2] and T W Zerda[1]

[1] Department of Physics and Astronomy, Texas Christian University, TCU 298840, Fort Worth, TX 76129, USA
[2] Institute of Physics, Nicolaus Copernicus University, ulica Grudziadzka 5/7, 87-100 Torun, Poland

Received 27 November 2007, in final form 22 April 2008
Published 9 July 2008
Online at stacks.iop.org/JPhysCM/20/325216

Abstract
SiC nanowires were produced from carbon nanotubes and silicon by two different methods at high temperature. X-ray powder diffraction was used to determine SiC concentration. The reaction rate using the Avrami–Erofeev method was determined for samples sintered at temperatures ranging from 1313 to 1823 K. The activation energy was found to be (254 ± 36) kJ mol^{-1}. The limiting factor in SiC formation is diffusion of silicon and carbon atoms through the produced layer of SiC.

1. Introduction

Silicon carbide is an important material, playing a key role in many fields. Production of silicon carbide wires of nanosize diameters is of interest because of the unique mechanical, optical, electronic, and other properties of these nanowires. There are three main growth mechanisms of SiC nanowires; (A) vapor–liquid–solid (VLS) [1, 2], (B) template-assisted growth from carbon nanotubes (CNTs) [3–6] and silicon nanowires [7], and (C) vapor–solid mechanism from nanostructured carbon particles [8, 9], silica [10], silicon [11], and silicon carbide [12]. The mechanism of formation of SiC nanowires from carbon nanotubes has not been fully characterized. Gorovenko *et al* [13] have investigated the high-temperature interaction in the silicon–graphite system. The process was a liquid-phase reaction, and the activation energy was determined to be 220 kJ mol^{-1}.

In this study we focus on SiC formation from carbon nanotubes and silicon. Due to the different hybridizations of carbon atoms there exist a large number of different phases of carbon, among which diamond and graphite are well known crystal forms. Fullerenes and CNTs are other forms of carbon and CNTs have been used to reinforce ceramic composites [14–19] including CNT/SiC composites [14, 19].

We studied the high-temperature reaction between multiwall CNTs and silicon. Here we describe the SiC fabrication process from CNTs that results in manufacturing SiC nanotubes and nanowires of diameters that depend on the sintering temperature. Scanning electron microscopy (SEM) was used to characterize the morphology of the nanostructures and x-ray powder diffraction (XRD) was used to determine SiC concentration. The activation energy was found by fitting data obtained from the Avrami–Erofeev equation. In the last section of this paper we discuss the mechanism of the reaction.

2. Sample preparation

Precursors for the samples were silicon powder with average particle size of 30 nm and multiwall carbon nanotubes with mean outer diameters (46 ± 18) nm and length 5–15 μm, purchased from Nanostructured and Amorphous Materials, Inc. There were two types of samples made.

The samples sintered in an induction furnace at various temperatures, referred to hereafter as induction furnace samples, were produced and analyzed to determine the activation energy. For these experiments the silicon nanopowder and carbon nanotubes were mixed, in a molar ratio of 2:1 Si:C, by dispersion in acetone and high energy sonication with an ultrasonic processor at 60 W. After mixing, the excess liquid was evaporated from the mixture at room temperature. The weight of each sample of the mixture was measured. The sample was poured into a tantalum crucible and then compressed with a small force. The crucible was placed on a ceramic stage inside a quartz tube (see figure 1) and the system was evacuated. During the sintering, vacuum better than 0.1 Pa (10^{-3} Torr) or 0.005 Pa (5.0×10^{-5} Torr) was maintained. Sintering of the mixture was done in an induction furnace using an Inductoheat Statipower BSP12 power supply with a custom-made coil. The quartz tube was held inside the cylindrical coil such that the sample was near the center of the coil. Most of the energy is lost to the tantalum by Joule

 © 2008 IOP Publishing Ltd Printed in the UK

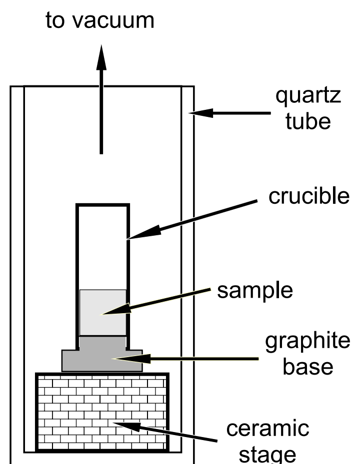

Figure 1. Schematic configuration of the sample, crucible, and isolating materials inside the quartz tube. The crucible was placed at the center of the induction coil.

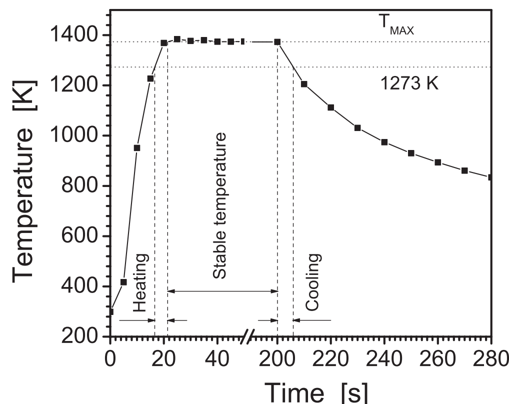

Figure 2. Schematic diagram of heating and cooling measurements. Temperature readings taken every 5 s provide accurate information for the error in measured reaction time.

heating which in turn heats the sample inside the crucible. The frequency was 25 kHz, and the current in the coil was adjusted to control the temperature of the sample inside. Temperature was measured by a thermocouple placed inside the crucible and inserted into the sample mixture. Only the crucible and its content were heated and reached high temperature. Of course radiation heating caused a modest increase of temperature of the quartz tube, but it never increased above 500 K. A couple of centimeters above the top of the crucible, the quartz was already at room temperature. This experimental setup ensured that no significant quantities of oxygen were released by the quartz tube. Also, by placing the crucible on the top of a graphite or steel base, which acted as oxygen scavenger, we further reduced the influence of oxygen on the mechanism of the reaction. No significant difference was noticed between experiments run at 10^{-3} Torr or 5×10^{-5} Torr, confirming our assumption that in this experimental setup, the effect of oxygen on the sintering process can be neglected. Therefore, most of the experiments were conducted at low vacuum conditions. In order to track the time of heating and cooling during the reaction, periodic temperature readings (every 5, 10 s, etc) were taken.

The other samples were sintered in a tube furnace. For the tube furnace experiments both powders were placed in separate boats and then placed in a quartz tube which was evacuated and sealed. The system was heated under vacuum conditions to 1473 K. Temperature was maintained constant for the duration of the sintering process. The preparation of these samples, which we will call tube furnace samples, was described in detail in our previous paper [5]. These samples were produced to study their morphology by transmission electron microscopy (TEM) and SEM and were not utilized to estimate the activation energy. Prior to SEM and TEM measurements, the tube furnace samples had been burned in air at 973 K for 2 h. The aim of this process was to remove any remaining unreacted carbon nanotubes.

3. Measurement procedure

The advantage to sintering by induction is that heating is fast, which reduces the error in measured reaction time. The sintering was run at the following temperatures: 1313, 1373, 1448, 1523, 1598, 1723, 1763, 1783, and 1823 K. At least five and up to 17 measurements were made for each sintering temperature.

Measurement of the reaction time was more precise than for the tube furnace samples, but because of gradual heating and then cooling of the samples, there was still significant error in determining the reaction time (see figure 2) especially for short times and high temperatures.

To improve our determination of the reaction time, we looked for the sintering temperature at which SiC formation starts. We found that no reaction occurred below 1273 K. This is in agreement with the observation by Teo and Sun [20] that SiC starts forming at $T > 1208$ K. In figure 2, this temperature is marked with a horizontal dotted line. The reaction time was determined as the stable temperature time plus half of the heating and cooling time above the minimum sintering temperature, 1273 K. The precision of the reaction time determined in this way is half of the heating and cooling temperature. The relative error is higher either for shorter times or for higher temperatures.

Each induction furnace sample was examined by XRD, which was used to determine the concentration of SiC. X-ray diffractograms were obtained on a Phillips PW2773 diffractometer, with Cu Kα radiation, $\lambda = 1.54$ Å. Figure 3 shows how the SiC(111) peak ($2\theta \sim 35°$) increases while the Si(111) peak ($2\theta \sim 28.5°$) decreases with longer sintering time. To determine the reaction rate for the produced silicon carbide, x-ray diffraction peaks (111) of SiC and (111) of Si were fitted using a Voigt profile. The intensities of fitted peaks were used to determine SiC mass concentration.

SEM images were obtained using a Hitachi S-4800 FE (field emission) scanning electron microscope, courtesy of Hitachi High Technologies in Dallas, Texas. Accelerating voltage ranged from 1 to 30 kV and magnifications ranging from ×4.0 to ×450 k were used in our analysis. In addition,

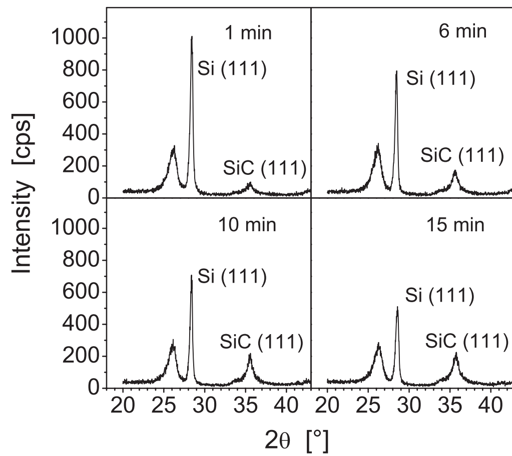

Figure 3. Comparison of SiC peak intensity as reaction time increases from 1 to 15 min.

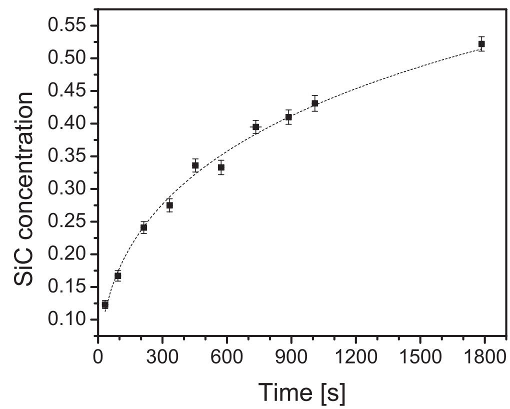

Figure 4. Graph of calculated SiC mass concentration versus reaction time for sintering at 1523 K. Data are fit to equation (3) the general reaction rate law from the Avrami–Erofeev model.

high resolution SEM images were taken on a Hitachi S-5500 FE scanning electron microscope, courtesy of Hitachi High Technologies in California.

4. Experimental results

The x-ray diffractograms of SiC produced from a mixture of silicon nanopowder and multiwall carbon nanotubes (both induction furnace and tube furnace samples) clearly indicated the presence of crystalline β-SiC with cubic symmetry, carbon nanotubes, and excess silicon (except for those samples for which the reaction was complete). After heating the samples at 973 K in air, peaks due to CNTs disappeared from the x-ray diffractograms and only peaks due to β-SiC and Si were present. No other crystalline structures were detected. It is evident that the burning procedure removes the remaining carbon nanotubes. Raman studies also showed that for those samples only peaks due to SiC and Si and no traces of carbon structures have been detected after the burning procedure. The relationship between x-ray peak intensity and mass concentration was found experimentally by measuring peak intensity for several known concentrations of silicon carbide and silicon mixtures. Pantea [21] made such measurements and found the following relation:

$$\alpha = 0.36x^2 + 0.64x \tag{1}$$

where α is the mass concentration of silicon carbide produced in the remaining silicon and silicon carbide, and x is the x-ray diffraction peak ratio of silicon carbide to the remaining silicon and silicon carbide as shown in equation (2).,

$$\alpha = \frac{m_{\mathrm{SiC}}}{m_{\mathrm{SiC}} + m_{\mathrm{Si}}} \qquad x = \frac{I_{\mathrm{SiC}}}{I_{\mathrm{SiC}} + I_{\mathrm{Si}}}. \tag{2}$$

Determination of the reaction rate is the first step in understanding the reaction mechanism. Oxygen involvement in the SiC formation process in the induction furnace samples was critically evaluated. High vacuum conditions, the presence of oxygen scavengers in close proximity to the precursors, and limiting high-temperature heating to the crucible and its content reduced the possibility that oxygen played a role in the SiC sintering. Furthermore, no SiO_2 was detected by x-ray and no Si–O bonds were present in the Fourier transform infrared (FTIR) spectra of the as-obtained specimens, prior to heating at 973 K to remove carbon. Also, a non-isothermal analysis based on the Friedman approach showed a linear dependence, indicating a single-stage process with an activation energy of about 250 kJ mol^{-1}. The experimental error was large and exceeded 50%. Therefore, to estimate the activation energy we applied the Avrami–Erofeev model.

The rate law for the reactions from the Avrami–Erofeev model has a general form given by:

$$-\ln(1-\alpha) = (kt)^n \tag{3}$$

where α is the fractional remains of the reactant on the interface and k is the rate constant of the chemical reaction, which is independent of concentration and time, but increases rapidly with increasing temperature. The value of the exponent n for one-, two- or three-dimensional reactions is in the range [0.5–1.5], [1.0–2.0], or [1.5–2.5], respectively [22].

In order to find the rate constant k and the exponent parameter n, data for SiC concentration and time of reaction were accumulated and plotted as shown in figure 4. A two-parameter fit to the equation then provides values of k and n for each specific temperature.

The results of the data fitting for each temperature are shown in table 1.

High error values in table 1 for 1783 K are due to the very small number (only three) of prepared samples. Once values of the reaction rate constant k are found for each temperature, the activation energy (E_a) can be found from the Arrhenius equation (equation (4)) by plotting $\ln k$ versus $1/T$ as shown in figure 5.

$$k = A\exp(-E_a/RT) \tag{4}$$

where E_a is the activation energy and R is the molar gas constant. The activation energy was found to be (254 ± 36) kJ mol^{-1}.

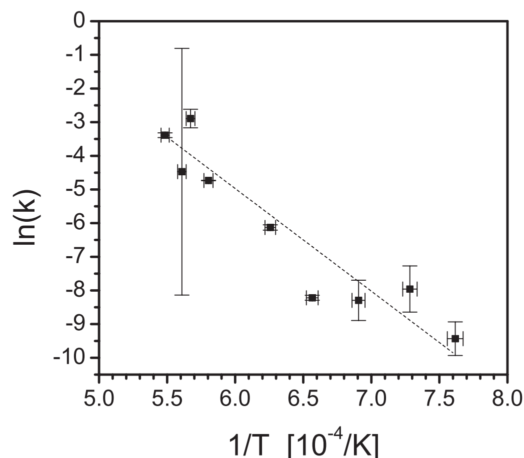

Figure 5. Fitting of Arrhenius equation (equation (4)). The very high error value for one point is connected to a small number of fitted points. The straight, dashed line is a result of linear fitting $\ln(k) = a(1/T) + b$ where $a = E_a/R$, R is the molar gas constant, and E_a is the activation energy.

Table 1. Results of two-parameter data fitting to the Avrami–Erofeev law to find the reaction rate constant k and parameter n for all temperatures.

T (K)	k ($\times 10^{-5}$)	n
1313 ± 10	8 ± 4	0.8 ± 0.9
1373 ± 10	35 ± 24	0.69 ± 0.21
1448 ± 10	25 ± 15	0.64 ± 0.15
1523 ± 10	27 ± 2	0.45 ± 0.02
1598 ± 10	218 ± 17	0.52 ± 0.04
1723 ± 10	879 ± 3	1.58 ± 0.03
1763 ± 10	5500 ± 1600	1.08 ± 0.21
1783 ± 10	1100 ± 4200	2 ± 20
1823 ± 10	3380 ± 240	1.16 ± 0.13

For the tube furnace samples, representative SEM pictures are shown in figure 6. From these and other images (not shown here) we measured diameters of nanotubes and the nanowires and then plotted their size distribution. Experimental data were fitted to log-normal distribution functions and the results are shown in figure 7. The mean diameter of sintered nanowires increased from 59 nm (reaction time—1 h) to 113 nm (after 6 h). Precursor CNTs had a mean diameter of (46 ± 18) nm.

After 1 h of sintering coaxial structures composed of SiC nanotubes on the outside and CNTs inside were produced. We estimate the thickness of SiC nanotubes from TEM images to be about 6 nm, compare figure 8. Previously, Menon *et al* [23] reported synthesis of SiC nanotubes and Wang *et al* [24] observed coaxial structures with the carbon core and SiC forming the shell. We concluded that after 1 h of sintering, a SiC layer coated the CNT and prevented oxygen from reaching the interior of the tube to react with carbon. For those samples, Raman spectra, in addition to SiC peaks, also showed peaks at 1580 and 1350 cm^{-1}, indicating the presence of carbon nanotubes. This result was confirmed by an FTIR study which also showed the presence of characteristic peaks due to carbon nanotubes (881 cm^{-1} [25], 1422 cm^{-1}, and 1643 cm^{-1} [26, 27]). However, for samples sintered in the tube furnace for times longer than 5 h and subsequently heated in air to 973 K, x-ray diffraction, Raman, and FTIR spectra did not show peaks characteristic of CNTs. These samples were solid wires.

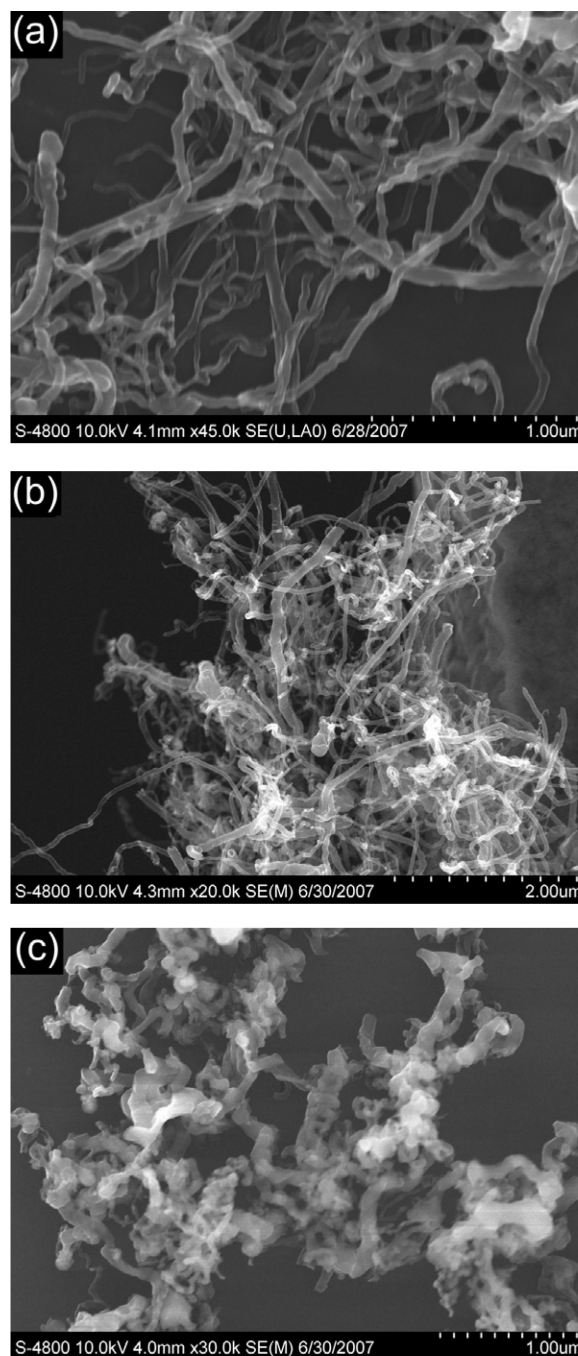

Figure 6. SEM pictures of: (a) pure multiwall CNTs, (b) SiC nanowires after 1 h of sintering, (c) SiC nanowires after 6 h of sintering.

Stacking fault formation can be observed in figure 8 as well. Examination of figures 6(a), (b) and 7 indicates that the SiC sample after 1 h sintering has the same morphology as the precursor CNTs but the SiC nanotubes have larger diameters. Since stacking faults are observed only in the crystal phase and not in amorphous SiC, we successfully

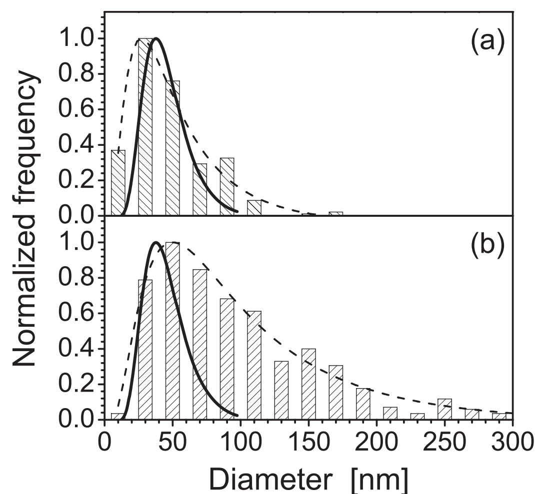

Figure 7. Fitting of the log-normal distribution function to the normalized distribution of SiC nanowire diameters: (a) SiC nanowires after 1 h of sintering. Mean diameter 59 nm and standard deviation 49 nm, (b) SiC nanowires after 6 h of sintering. Average diameter 113 nm and standard deviation 97 nm. The bold continuous line is for distribution of the precursor CNTs with average diameter (46 ± 18) nm.

Figure 8. High resolution SEM picture of SiC nanotubes obtained after 1 h of sintering at 1200 °C. Thickness of the SiC nanotubes walls is about 6 nm while the outer diameter is about 22 nm. Diagonal lines in the SiC phase are stacking faults.

produced nanosize crystalline tubes. After sintering for 6 h only solid SiC nanowires were observed (no SiC nanotubes). In comparison with the product sintered for 1 h, diameters of SiC nanowires were significantly larger. Silicon sublimes at low temperatures and at 1473 K its vapor pressure is about 1.3×10^{-1} Pa [28]. The reaction starts when silicon vapor reaches the CNT. Probably, the nuclei of the reaction are the Stone–Wales defects on the outer layers of the carbon nanotubes [6]. The reaction then proceeds along the nanotubes and at this stage it is controlled by surface diffusion of silicon [29]. The observed radial growth of SiC on the CNT requires silicon to diffuse through the produced SiC layer toward CNTs or diffusion of carbon from the inside to the outside of the boundary phase SiC layer. Diffusion coefficients of both atoms in crystalline SiC are very small [30], and to explain the rapid

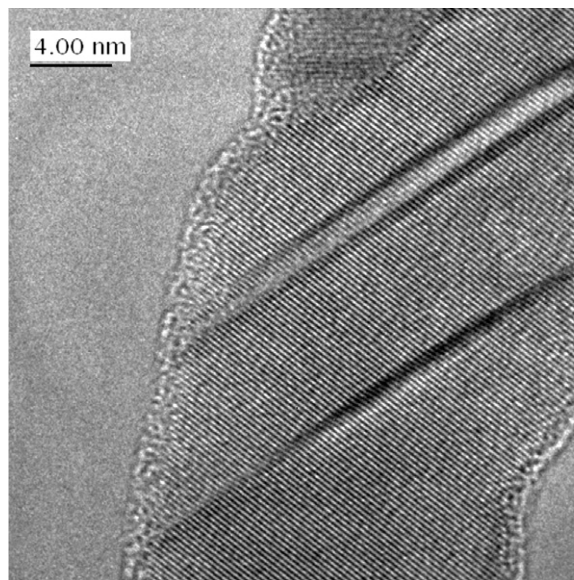

Figure 9. High resolution TEM picture of SiC nanowire obtained after 64 h of sintering in 1200 °C. Amorphous SiO_2 formed during postproduction heat treatment is seen as a 1–2 nm thick layer coating the nanowire. Diagonal lines are stacking faults [5].

growth of SiC we assume that it proceeds mainly by diffusion of those atoms along grain boundaries and along stacking faults and dislocations. Because the energy of activation determined in this study is similar to that observed during the SiC growth on diamonds or graphite, we postulate that the diffusion of silicon and carbon atoms controls the rate of SiC growth. Previously we studied defects in nanosize SiC and noted an abundance of stacking faults in nanosize SiC, especially in SiC nanowires [5, 6, 31].

This mechanism of formation of nanowires leads to the conclusion that the process is governed by diffusion. It is possible that interlayer spacing in SiC nanotubes is different from that in bulk SiC, however, the precision of our measurements was not sufficient to make such a determination. As silicon diffuses into the interior of the coaxial structure it transforms carbon nanotubes into SiC and eventually the interior becomes solid SiC. The outer diameter of the nanowires also grows, indicating that carbon atoms continue to diffuse through the SiC layers. There is evidence that the outermost layers of our produced SiC nanowires are amorphous silica (compare figure 9). This silica layer was formed during the burning of the remains of carbon in air, which was confirmed by IR spectra recorded before and after burning. A peak centered at about 1100 cm^{-1} and assigned to Si–O vibrations was clearly noticed in all samples heated to 973 K.

In previous research done by our group, we studied SiC formation from precursors diamond and silicon under high-pressure high-temperature conditions. We found activation energies ranging from 170 kJ mol^{-1} for nano-diamond to 260 kJ mol^{-1} for micro-diamond [32]. Our value of the activation energy for the reaction between silicon nanopowder and CNTs, (254 ± 36) kJ mol^{-1}, is in good agreement with those obtained by Pantea *et al* [21, 32] for the diamond–silicon

reaction. Our previous results for sintering SiC nanowires from the same precursors under high pressure (2 GPa) showed the activation energy was (96 ± 29) kJ mol^{-1} [6]. The reduced energy of activation observed for the reaction run under high-pressure conditions further indicates that the limiting factor is the diffusion of atoms through the SiC layer. Increased pressure increases the population of defects and enlarges the volume of grain boundaries, thus enabling faster diffusion of atoms.

Intermediate results of n show that the reaction mechanism is probably diffusion-controlled one-dimensional growth with a decelerating nucleation rate. It is worth mentioning that this is true up to the temperature 1598 K. The significant change in the value of n starting from 1723 K leads to the conclusion that, beginning at this temperature two-dimensional growth is observed. Indeed we noticed that at higher temperatures, individual nanowires fuse together to form planar structures.

5. Summary

In this study we discuss the reaction between silicon and multiwall carbon nanotubes. Initially, the outer layers of the carbon multiwall nanotubes are transformed into SiC nanotubes while the inner region of the nanotubes remains unchanged. The SiC nanotubes are precursors of solid SiC nanowires. With elapsed sintering time silicon and carbon diffuse through the produced SiC layers mainly along the stacking faults and grain boundaries such that SiC grows layer by layer. There is evidence of amorphous SiC and SiO_2 formation on the outermost layers after long sintering times. The activation energy, (254 ± 36) kJ mol^{-1}, obtained from this experiment is in good agreement with previous studies on SiC growth in which diffusion of silicon and carbon was also the limiting factor.

Acknowledgments

This study was partially supported by NSF grant DMR 0502136 and TCU RCAF fund.

References

[1] Zhou X T, Lai H L, Peng H Y, Au F C K, Liao L S, Wang N, Bello I, Lee C S and Lee S T 2000 *Chem. Phys. Lett.* **318** 58–62
[2] Zhang H F, Wang C M and Wang L S 2002 *Nano Lett.* **2** 941–4
[3] Daï H, Wong E W, Lu Y Z, Fan S and Lieber C M 1995 *Nature* **375** 769–71
[4] Zhang Y, Ichihashi T, Landree E, Nihey F and Iijima S 1999 *Science* **285** 1719
[5] Wallis K L, Wieligor M, Zerda T W, Stelmakh S, Gierlotka S and Palosz B 2007 *J. Nanosci. Nanotechnol.* **8** 3504–10
[6] Wang Y and Zerda T W 2006 *J. Phys.: Condens. Matter* **18** 2995
[7] Zhang Y F, Tang Y H, Zhang Y, Lee C S, Bello I and Lee S T 2000 *Chem. Phys. Lett.* **330** 48–52
[8] Meng G W, Cui Z, Zhang L D and Philipp F 2000 *J. Cryst. Growth* **209** 801–6
[9] Bechelany M, Brioude A, Stadelmann P, Ferro G, Cornu D and Miele P 2007 *Adv. Funct. Mater.* **17** 3251–7
[10] Wu X C, Song W H, Zhao B, Huang W D, Pu M H, Sun Y P and Du J J 2000 *Solid State Commun.* **115** 683–6
[11] Saulig-Wenger K, Cornu D, Chassagneux F, Ferro G, Epicier T and Miele P 2002 *Solid State Commun.* **124** 157–61
[12] Yang W, Araki H, Hu Q, Ishikawa N, Suzuki H and Noda T 2004 *J. Cryst. Growth* **264** 278–83
[13] Gorovenko V I, Knyazik V A and Shteinberg A S 1993 *Ceram. Int.* **19** 129
[14] Ma R Z, Wu J, Wei B Q, Liang J and Wu D H 1998 *J. Mater. Sci.* **33** 5243
[15] An J-W, You D-H and Lim D-S 2003 *Wear* **255** 677
[16] Peigney A, Flahaut E, Laurent C, Chastel F and Rousset A 2002 *Chem. Phys. Lett.* **352** 20
[17] Balazsi C, Konya Z, Weber F, Biro L P and Arato P 2003 *Mater. Sci. Eng.* C **23** 1133
[18] Zhan G-D, Kuntz J D, Wan J and Mukherjee A K 2003 *Nat. Mater.* **2** 38
[19] Wang Y, Voronin G, Zerda T W and Winiarski A 2006 *J. Phys.: Condens. Matter* **18** 275–82
[20] Teo B K and Sun X H 2007 *Chem. Rev.* **107** 1485
[21] Pantea C 2004 Kinetics of diamond–silicon reaction under high pressure–high temperature conditions *PhD Thesis* Texas Christian University
[22] Hulbert S F 1969 *J. Br. Ceram. Soc.* **6** 11
[23] Menon M, Richter E, Mavrandonakis A, Froudakis G and Andriotis A N 2004 *Phys. Rev.* B **69** 115322
[24] Wieligor M, Wang Y and Zerda T W 2005 *J. Phys.: Condens. Matter* **17** 2387–95
[25] Kim U J, Liu X M, Furtado C A, Chen G, Saito R, Jiang J, Dresselhaus M S and Eklund P C 2005 *Phys. Rev. Lett.* **95** 157402
[26] Dillon A C, Gennett T, Alleman J L and Jones K M 2000 *Proc. 2000 DOE/NREL Hydrogen Program Review (May)*
[27] Misra A, Tyagi P K, Singh M K and Misra D S 2006 *Diamond Relat. Mater.* **15** 385
[28] Nesmeyanov A N 1963 *Vapour Pressure of the Elements* (New York: Academic)
[29] Sun X H, Li C P, Wong W K, Wong N B, Lee C S, Lee S T and Teo B K 2002 *J. Am. Chem. Soc.* **124** 14464
[30] Cimalla V, Wohner Th and Pezoldt J 2000 *Mater. Sci. Forum* **338–342** 321
[31] Gubicza J, Nauyoks S, Balogh L, Zerda T W and Ungár T 2007 *J. Mater. Res.* **22** 1314–21
[32] Pantea C, Voronin G A, Zerda T W, Zhang J, Wang L, Wang Y, Uchida T and Zhao Y 2005 *Diamond Relat. Mater.* **14** 1611–5